

***In situ* formation of TiC particulate composite layer on cast iron by laser alloying of thermal sprayed titanium coating**

HEUNG-IL PARK

Department of Production and Joining Eng. of Pukyong National University, Pusan, 608-739, Korea

KAZUHIRO NAKATA

Joining and Welding Research Institute of Osaka University, Ibaraki-shi, Osaka, 567, Japan

SHOGO TOMIDA

Toyama Industrial Technology Center, Takaoka-shi, Toyama, 933, Japan

E-mail: pnwpark@pine.pknu.ac.kr

Commercial flake graphite cast iron substrate was coated with titanium powder by low pressure plasma spraying and was irradiated with a CO₂ laser to produce the wear resistant composite layer. The macro and microstructural changes of an alloyed layer with the traveling speeds of laser beam, the precipitate morphology of TiC particulate and the hardness profile of the alloyed layer was examined. From the results, it was possible to composite TiC particulate on the surface layer by direct reaction between carbon existed in the cast iron matrix and titanium with thermal sprayed coating by remelting and alloying them using laser irradiation. The cooling rate of the laser remelted cast iron substrate without a titanium coating was about 1×10^4 K/s to 1×10^5 K/s in the order under the condition of this study. The microstructure of the alloyed layer consisted of three zones; the TiC particulate precipitate zone (MHV 400–500), the mixed zone of TiC particulate + ledeburite (MHV 650–900) and the ledeburite zone (MHV 500–700). TiC particulates were precipitated as a typical dendritic morphology. The secondary TiC dendrite arms were grown to a polygonized shape and were necking. Then the separated arms became cubic crystal of TiC at the slowly solidified zone. In the rapidly solidified zone near the fusion boundary, however the fine granular TiC particulates were grouped like grapes.

© 2000 Kluwer Academic Publishers

1. Introduction

The advantages of cast iron as an engineering material is that it can be used to produce complex shaped parts economically because of good castability and it has good machinability and lubrication property etc. The cast iron can be classified as graphite composite which contains 10 volume percentage of carbon in the steel matrix [1].

Laser surface alloying is a beneficial surface modification process to achieve functionality, to improve the strength and hardness and to make a composite layer in a material surface [2, 3]. There are several methods of adding an alloy element for surface alloying, they are, pre-coating of an alloy element to the matrix, cladding, gas method, direct addition of alloying powder to the remelted surface and wire addition [4–8].

Laser surface modification for the cast iron can be divided into two processes; the heating process where the surface was heated up to the beneath of melting point and the remelting process where the surface was remelted and alloyed. Self-diffusion quenching occur

in the last stage of these processes. The heating process includes hard eye treatment of cast iron [9] and hardening of the cylinder liner [10] or piston ring [11] for diesel engines. Remelting and rapid cooling treatment of the surface of the cam shaft or rocker arm [12] and alloying a small amount of chrome for valve seat [11] are classified as the melting process. These processes increase the wear resistance of cast iron by self-diffusion quenching, the formation of hard phase by remelting or surface alloying.

Production of *in situ* carbide-reinforced composites by solidification processing would be one of the simplest techniques to produce MMCs. It is expected to make a hard carbide particulate composite on a cast iron surface by alloying carbide former element such as titanium and reacting *in situ* with carbon contained in cast iron. However, there is limited research on this process [13, 14] and more efforts are required.

In this study, low pressure plasma thermal spraying under a non-oxidizing atmosphere was used to make a dense titanium coating prior to laser irradiation. To

examine the possibility of *in situ* formation of the TiC particulate composite layer, CW CO₂ laser was irradiated on the titanium coating of the cast iron substrate. The effect of the traveling speed of the laser beam on the solidification microstructure of the base metal and titanium alloyed beads were examined. The precipitation morphology of TiC particulate generated by the reaction with carbon contained in the cast iron matrix and the hardness profile in the titanium alloyed layer were also observed.

2. Materials and experimental procedures

Table I shows a chemical composition of cast iron used in this study and the size and chemical composition of titanium powder. Flake graphite cast iron was cast into a sand mold with dimensions of 100 × 120 × 10 mm and machined to the plate with dimensions of 50 × 60 × 6 mm. The spray powder was a commercial product (Showa Denko Ltd.) manufactured in the air and had a size distribution of -45 ~ +10 μm (Fig. 1A). The surface of the cast iron plate was cleaned using acetone and was blasted with alumina to improve the bonding strength of sprayed coating.

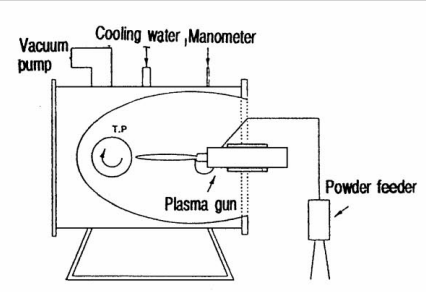
The conditions of low pressure plasma spraying and surface alloying by CW CO₂ laser processing are shown in Table II. For convenience, specimens designated as Gxx and GTxx, where G refers to gray cast iron substrate without coating, GT the specimens with a titanium coating and XX the traveling speed of laser beam. To obtain a dense coating and prevent oxidation of the titanium powder during thermal spraying, a plasma sprayer (METEKO 7MB, 80 kW) was used under low pressure (5.2×10^4 Pa) and a titanium coating of 200 μm in thickness was formed on the cast iron plate (Fig. 1B). Argon and hydrogen gases were used as primary and secondary gases respectively. Surface alloying of the titanium was carried out by irradiating CW CO₂ laser beam (MITSUBISHI 25C) at the conditions of the laser output 2300 W, defocusing distance +50 mm and a scanning width 5 mm. The remelting bead of 50 mm in length was produced with different traveling speeds of 0.83, 1.67, 3.33 and 5.00 mm/s of laser beam. The surface alloyed specimen was heat-treated in a vacuum furnace (6.7×10^{-3} Pa, 1223 K, 10.8 ks) and cooled for comparing as-alloyed specimen. Microstructure was observed using an optical microscope

TABLE I Chemical compositions of materials used

Materials		Chemical compositions (mass%)							Remarks	
Base metal	C	Si	Mn	P	S	—	—	—	Sand casting: 100 × 120 × 10 (mm) Specimen size: 50 × 60 × 6 (mm)	
	3.4	1.8	0.8	0.08	0.08	—	—	—		
Ti-powder	Ti	Fe	Si	Cl	N	C	H	O	Commercial powder: Showa Denko Ltd. Grain size: -45 ~ +10 (μm)	
	Bal.	0.02	0.004	0.02	0.03	0.004	0.015	0.42		

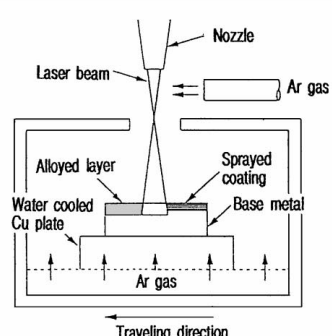
TABLE II Conditions of low pressure plasma spraying [LPPS] and laser surface alloying

Low pressure plasma spraying	
Pressure(Pa)	5.2×10^4
Primary gas	Ar
Pressure(Pa)	1.3×10^4
Flow rate(m ³ /s)	8.0×10^{-4}
Secondary gas	H ₂
Pressure(Pa)	0.78×10^4
Flow rate(m ³ /s)	1.44×10^{-4}
Plasma conditions	
Arc current(A)	500
Arc voltage(V)	60
Spraying distance(mm)	250



Plasma gun : METEKO 7MB

CO ₂ laser processing	
Power(W)	2300(multi mode)
Traveling speeds(mm/s)	0.83, 1.67, 3.33, 5.00
Defocused distance(mm)	+50
Scanning frequency(Hz)	100
Scanning width(mm)	5
Shield gas	Ar



CO₂ laser : MITSUBISHI 25C

Specimen symbols				
Groups	Traveling speeds(mm/s)			
	0.83	1.67	3.33	5.00
Base metal	G50	G100	G200	G300
Ti-coated	GT50	GT100	GT200	GT300

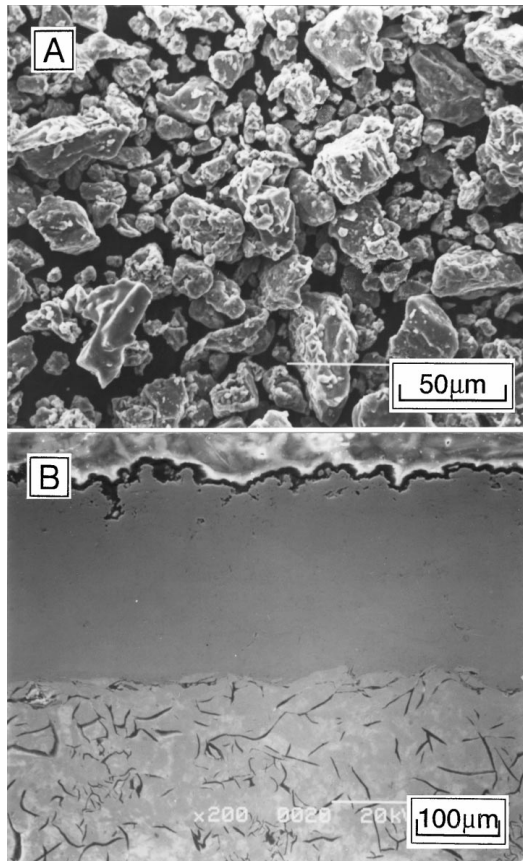


Figure 1 SEM morphology of titanium powder (A) and titanium coating on the cast iron substrate by low pressure plasma spraying (B).

and scanning electron microscope (SEM), electron probe microanalysis (EPMA) and X-ray diffraction analysis (XRD) were performed. Microhardness testing was also carried out. The cooling rate of the remelted

bead at different traveling speeds was estimated by observing the microstructure of the cast iron matrix without a titanium coating.

3. Results and discussion

3.1. Cooling rates of the laser remelted cast iron substrate

Fig. 2 shows the microstructural changes of the remelted cast iron substrate without titanium coating at different traveling speeds. The microstructure of the remelted cast iron matrix showed the fine ledeburite. Dendrite arm spacings (λ) of ledeburite were 1.54, 1.25, 1.05 and 0.85 μm at traveling speeds of 0.83(G50), 1.67(G100), 3.33(G200) and 5.00 mm/s(G300), respectively. Fig. 3 shows the calculated cooling rate of the remelted substrate for the traveling speed of the laser beam by substitution of λ measured in this study to the experimental equation of Kurobe which was derived from the cooling rate after surface remelting using a CO_2 laser in the Fe-3mass%C-2mass%Si alloy [15]. The calculated values were 1.15×10^4 K/s and 10.97×10^4 K/s at traveling speeds of 0.83 and 5.00 mm/s respectively. As a result, the cooling rate of the remelted bead, in cast iron, in this study was assumed to be about 1×10^4 K/s to 1×10^5 K/s.

3.2. Surface appearance of alloyed bead and its macrostructures

Fig. 4 shows the variation of surface appearances and cross-sectional macrostructures of the titanium alloyed bead at the different traveling speeds. All beads show severe surface ripple. A few small pores are shown

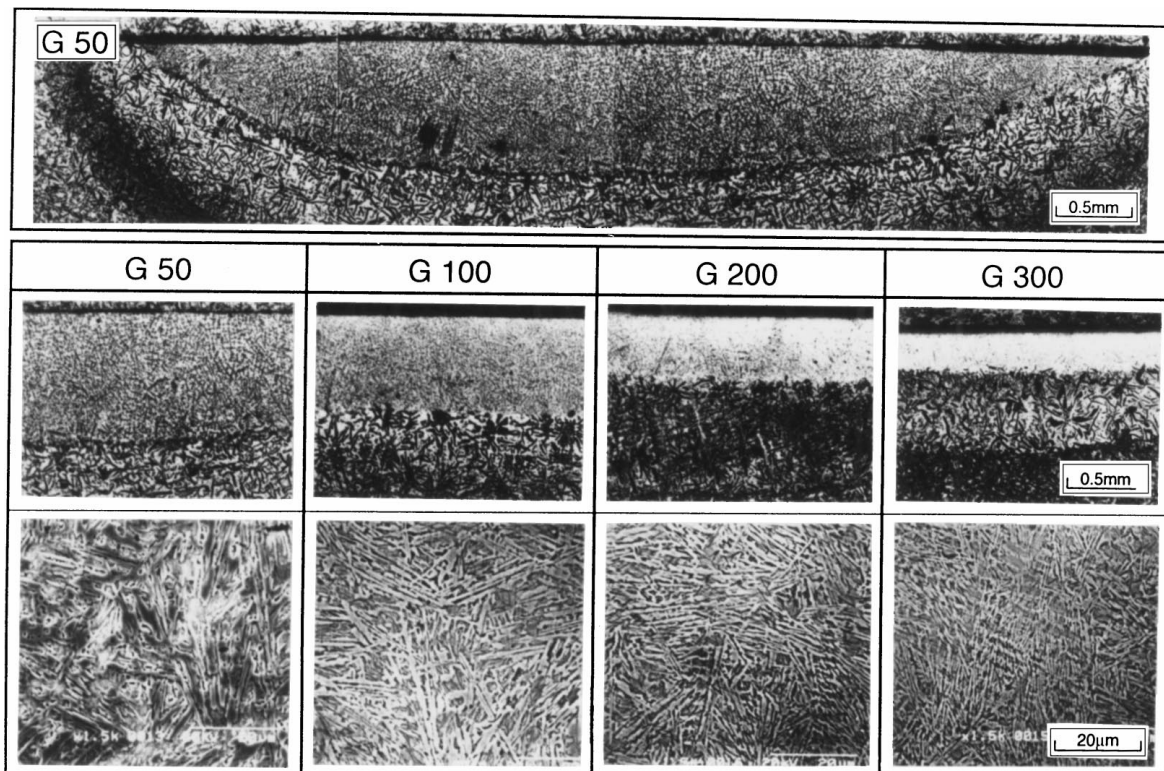


Figure 2 Microstructural changes of laser remelted cast iron substrate with the traveling speeds of laser beam.

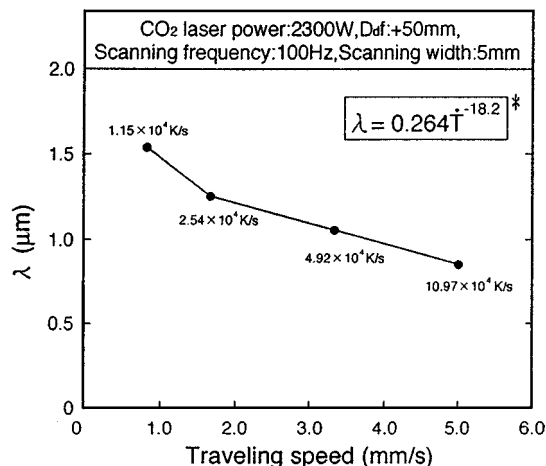


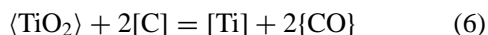
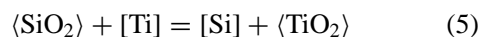
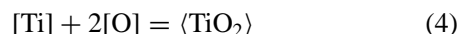
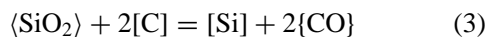
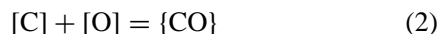
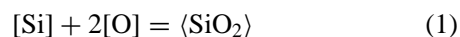
Figure 3 Secondary dendrite arm spacing (λ) and calculated cooling rate of laser remelted cast iron substrate with the traveling speeds of laser beam.

in the beads with traveling speeds of 0.83 mm/s and 1.67 mm/s, while large pores are shown in the beads with speeds of 3.33 mm/s and over. Especially, sponge-like pores are shown in the entire surface of beads with traveling speeds of 5.0 mm/s. In the case of GT50 and GT100 a few pores are shown in the surface of bead, but a lot of pores still present inside of those bead. Large pores were observed in the fusion boundary and small pores were observed in the slowly solidified zone in the center of bead.

Surface ripples of the bead were closely related to the temperature gradient or surface tension gradient [16]. The macrostructure of the bead without alloying showed a few pores and a smooth bead surface (see Fig. 2). The titanium alloyed bead was less smooth than

the bead without alloying in cast iron. These phenomena were assumed to be due to the decreased fluidity by the formation of TiC in titanium alloyed molten pool as later discussed.

The main alloying elements in cast iron are carbon and silicon. The following redox reactions are possible during alloying of coated titanium on cast iron;



Since cast iron is melted in air, more oxygen than equilibrium content can be introduced to the melt from the atmosphere. By the oxidation of cast iron melt ($\langle \text{SiO}_2 \rangle$) was generated in accordance with Equation 1 in temperatures below 1673 K and $\{\text{CO}\}$ was formed by Equation 2 in temperatures over 1673 K [17]. Generally, gray cast iron is melted below 1673 K and then heated up above 1773 K just before tapping. Therefore, when cast iron is melted to over 1673 K, $\langle \text{SiO}_2 \rangle$ suspended in the melt is reduced by $[\text{C}]$ with Equation 3 and then only small amount of $\langle \text{SiO}_2 \rangle$ is remained in the melt.

If cast iron is welded in air, the $\langle \text{SiO}_2 \rangle$ which was suspended in the matrix or formed by the reaction with oxygen from the atmosphere should be reduced by carbon in the matrix itself to generate $\{\text{CO}\}$ gases. Pores can be formed when this $\{\text{CO}\}$ gas is captured in the weld pool [18].

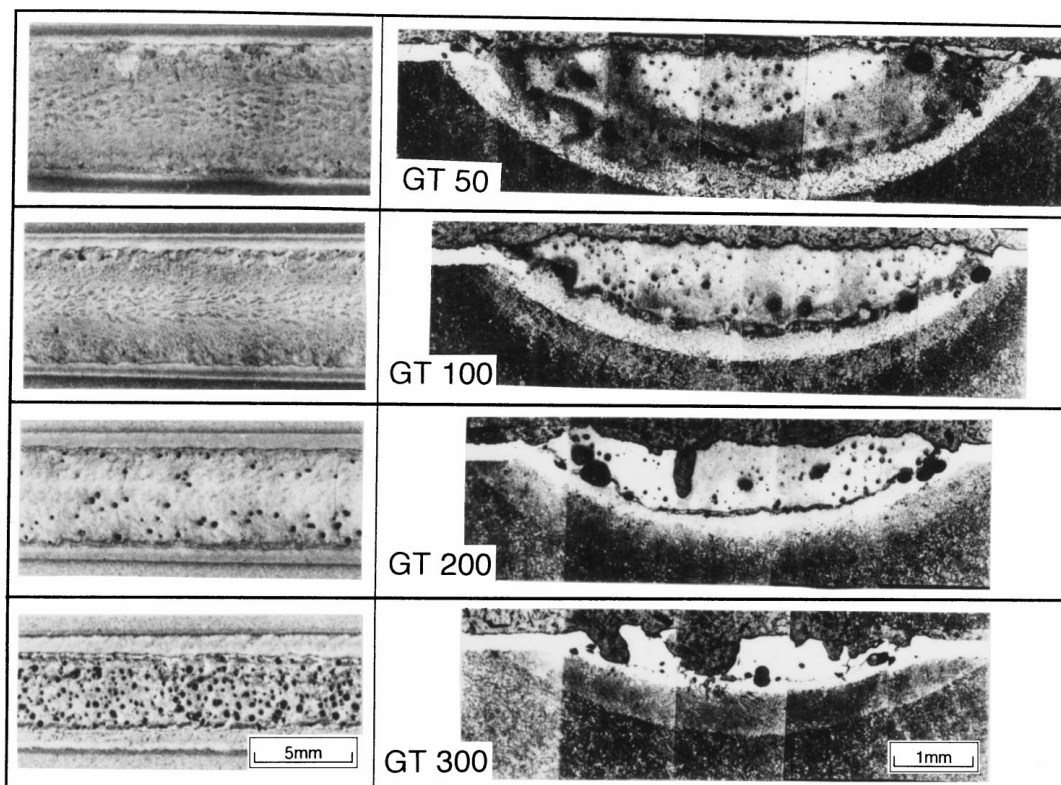


Figure 4 Surface appearance of titanium alloyed bead and its sectional macrostructure with the traveling speeds of laser beam.

No pores are shown in the bead without titanium alloying as see Fig. 2 indicates that the effect of $\langle \text{SiO}_2 \rangle$ reduction in the matrix is negligible and the formation of $\langle \text{SiO}_2 \rangle$ is restricted due to the argon atmosphere. However, a lot of pores are shown in the titanium alloyed bead. If $\langle \text{SiO}_2 \rangle$ is present in the cast iron matrix, $\langle \text{SiO}_2 \rangle$ should be reduced by titanium to form $\langle \text{TiO}_2 \rangle$ according to Equation 5 during surface alloying process because titanium-oxide has negative standard free energy of formation than silicon-oxide [19]. $\langle \text{TiO}_2 \rangle$ should in turn be reduced by carbon in the matrix to evolve $\{\text{CO}\}$ gases with Equation 6. If the formation of $\langle \text{SiO}_2 \rangle$ is restricted as in the bead without alloying titanium, the formation of pores in the titanium alloyed bead is regarded as a consequence of Equation 6. The titanium powder used in this study has a large amount of oxygen as shown in Table I, titanium could react with oxygen to form $\langle \text{TiO}_2 \rangle$ during plasma spraying. Consequently, the $\langle \text{TiO}_2 \rangle$ that existed in the molten pool should be reduced by the carbon to generate $\{\text{CO}\}$ gas. This $\{\text{CO}\}$ gas also contributed to the formation of pores when it was captured in the weld pool. In fact $\langle \text{TiO}_2 \rangle$ was detected from the X-ray diffraction analysis on the titanium alloyed layer of GT50 (see Fig. 8). On the other hand, the GT300 specimen showed sponge-like pores in the surface and bead inside. It is assumed that the pores were trapped in the bead by rapid cooling of weld pool, and on the contrary at the lower cooling rate in GT50 they easily escaped from the weld pool surface.

Fig. 5 shows the changes of the width and melt depth of the bead at different traveling speeds when the cast iron was alloyed with titanium. In the titanium coated cast iron, the melt depth of the bead was 2.2 times thicker than that of the cast iron without a titanium coating at a traveling speed of 0.83 mm/s and 2.7 times thicker at 5.0 mm/s. However, the bead width was not changed significantly in both cases (1.2 times and 1.0 times width at 0.83 mm/s and 5.0 mm/s respectively). When the as-blasted cast iron is remelted by the laser, there was a severe reflection of the beam and lens contamination was observed. Consequently, the increased melt depth of the bead in the titanium coated

cast iron was attributed to the increased rate of laser beam absorption due to the titanium coat [8]. The bead width was restricted by the beam oscillation width.

3.3. Microstructures of alloyed layer

Fig. 6 shows optical and SEM micrographs of the bead section in GT50. The specimen was etched with 4% nital. The titanium alloyed zone and ledeburite zone were clearly observed in the microstructure of bead section. The SEM micrograph shows that polygonic particulates up to $6 \mu\text{m}$ in size were precipitated in the top part of bead (Fig. 6A) where the cooling rate was the slowest, and fine granular particulates under $2 \mu\text{m}$ in size tended to be precipitated near the boundary of ledeburite zone (Fig. 6B).

Fig. 7 shows the EPMA line analysis about carbon and titanium in the same bead section. Carbon and titanium were detected in the alloyed zone where the particulates were precipitated. However titanium was not detected in the ledeburite zone. By the X-ray diffraction analysis the alloyed bead section consisted of TiC , TiO_2 , Fe_3C and $\alpha\text{-Fe}$ (see Fig. 8). These observations clearly show that TiC particulates can be made by a direct reaction between carbon and titanium and TiC precipitated layer can be made in the cast iron surface by laser surface alloying of titanium which is thermal sprayed on the cast iron in advance.

On the other hand, in the microstructure of the bead section in Fig. 4 and Fig. 6, the boundary between the titanium alloyed zone and ledeburite zone was irregular, while the boundary between the ledeburite zone and base metal was clearly visible as a half circle. The melt in the weld pool shows two types of fluid flow as a result of the thermal gradient [2]. One is center-to-side motion that it moves to the bottom of the bead through the side of the bead where the temperature is relatively low, reached the bottom center and then back to the surface highest temperature area near heat source. The other is a front-to-back motion that moves in a reverse direction to the heat flow. Such motions of melt are shown in the solidification microstructure of the bead which reveals

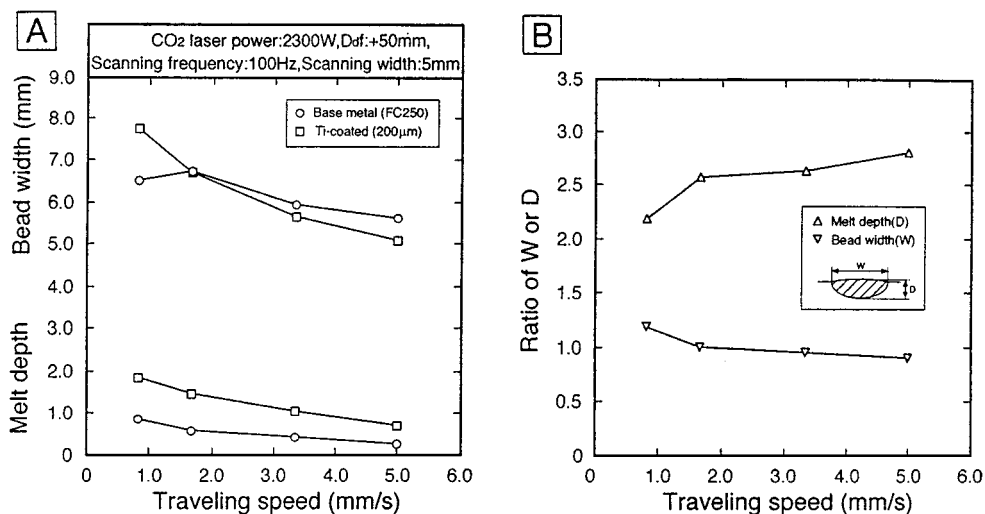


Figure 5 Effects of titanium coating and the traveling speeds on the bead width and melt depth (A), and ratio of bead width or melt depth (Ti-coated/base metal) (B).

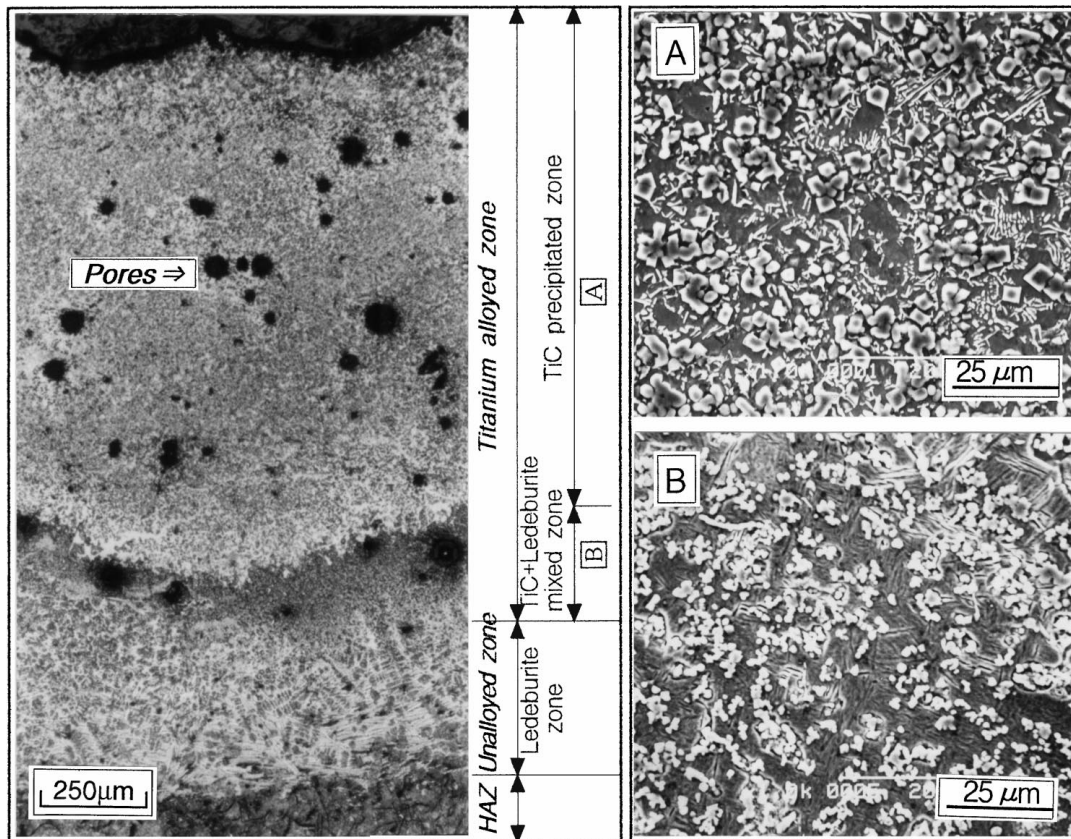


Figure 6 Optical and SEM micrographs of titanium alloyed bead section (GT50), 4% nital etched. (A): TiC precipitated zone, (B): TiC + ledgeburite mixed zone.

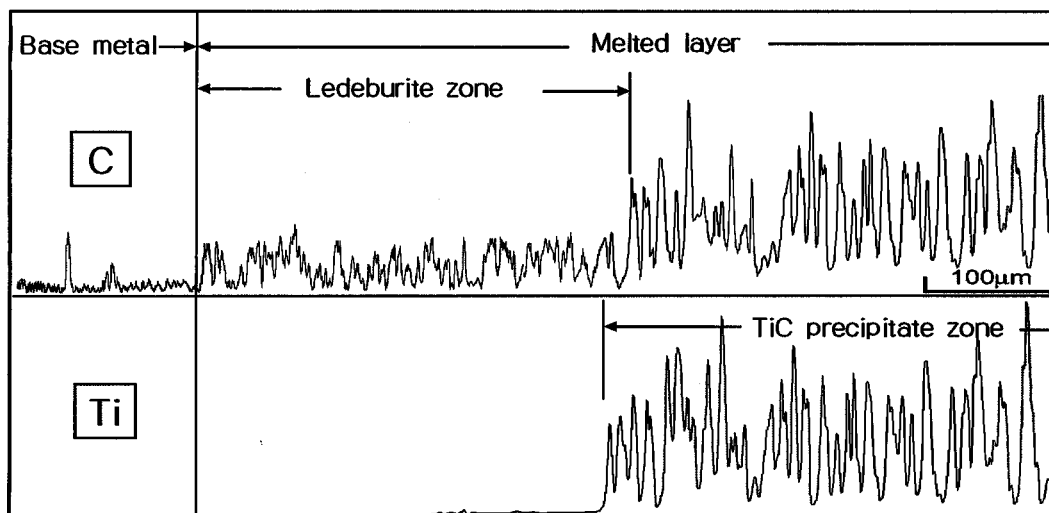


Figure 7 EPMA depth profile of carbon and titanium elements for titanium alloyed bead section (GT50).

the trace of alloying phenomena. As shown in Fig. 6, it was found that these convective motions have a large effect on the mixing process of the titanium coat into the molten pool.

The boundary between the ledgeburite zone and the base metal was, however, clearly distinguished as a half circle unlike the boundary between the TiC precipitate zone and ledgeburite zone. This finding means that remelting of the lower melting point base metal was continued during solidification of the titanium alloyed molten pool. The remelted base metal near the fusion boundary rapidly solidified to form a ledgeburite structure and produced a clear half circle boundary defined

only by the temperature distribution. This microstructure was also observed when the cast iron was welded with the nickel base electrode [20].

Based on the above discussion, it is clear that the laser alloyed bead section consisted of three zones; the titanium alloyed zone where the fine TiC particulates were precipitated, partial titanium alloyed zone where TiC particulates were mixed with ledgeburite which was remelted and solidified in the early stage of heating, and the ledgeburite zone where it was formed by partial remelting and solidification of cast iron matrix adjacent to the base metal during solidification of the alloyed weld pool with the moving heat source.

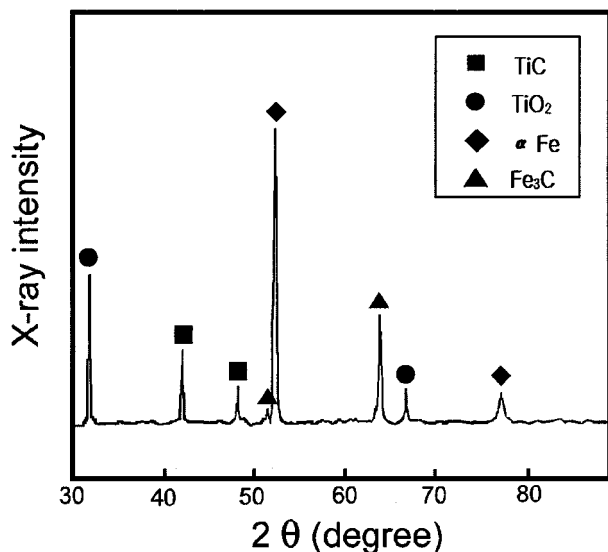


Figure 8 X-ray diffraction pattern of the titanium alloyed zone (GT50).

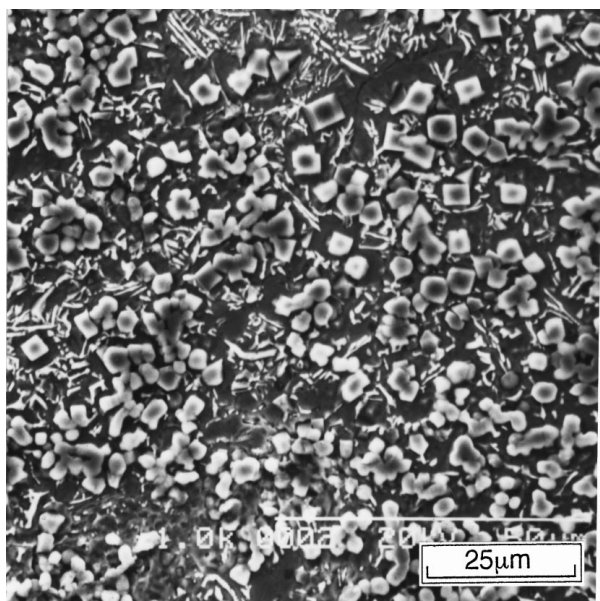


Figure 9 SEM micrograph of TiC composite layer by laser surface alloying of titanium (GT50).

3.4. Morphology of TiC particulate

Fig. 9 shows the SEM morphology where the TiC particulate composited in the titanium alloyed layer of a GT50 specimen. Fig. 10 shows the results of EPMA area analysis about elements [Fe], [Ti], [C], [Si] and [O] in the same area of Fig. 9. Titanium and carbon were detected in the polygonic or granular particulates precipitated to the titanium alloyed zone, while iron and silicon were detected only in the matrix. Especially, titanium, carbon and oxygen were detected simultaneously in the central area where the fine TiC particulates were grouped. The existence of TiO₂ oxides were confirmed by X-ray diffraction analysis in the same area of alloyed bead. In addition to this, the EPMA area analysis confirmed the existence of oxygen in the center of the grouped TiC particles. Therefore, it is assumed that the suspended TiO₂ formed in the weld pool act as the nucleation site of TiC dendrite.

Fig. 11 shows a SEM micrograph of the microstructure of TiC particulate deeply etched by the mixed solution of HNO₃ + HF + H₂O from the same specimen. TiC particulates were precipitated as the typical dendritic morphology in the upper part of the bead because of the reduced solidification rate (Fig. 11A, B). Fine granular TiC particulates were grouped like grapes within ledeburite which being close to the fusion boundary because of fast solidification rate (Fig. 11C, D). If severe thermal and compositional convections exist in the melt, dendrites will grow irregularly, since dendrite arms grow by avoiding regions with larger solute segregation [21]. Fig. 11B also shows the growth and separation of secondary dendrite arm. The root of the secondary TiC dendrite arm was necking and the arm was also growing to the polygonic crystal and then became cubic crystal of TiC.

Fine polygonic, cubic or granular particulates found in Fig. 10 were TiC particulate precipitated in the dendritic morphology. As the TiC particulates are combined to each other in the dendritic morphology in the TiC alloyed layer, TiC particulates can be difficult to

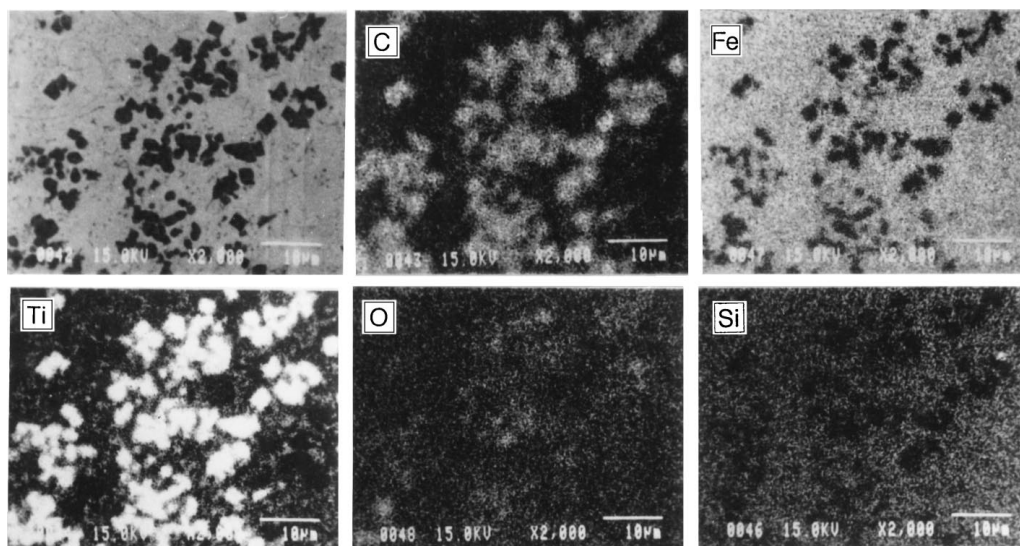


Figure 10 EPMA area analyses on the elements [C], [Fe], [Ti], [O] and [Si] in the same composite layer of Fig. 9.

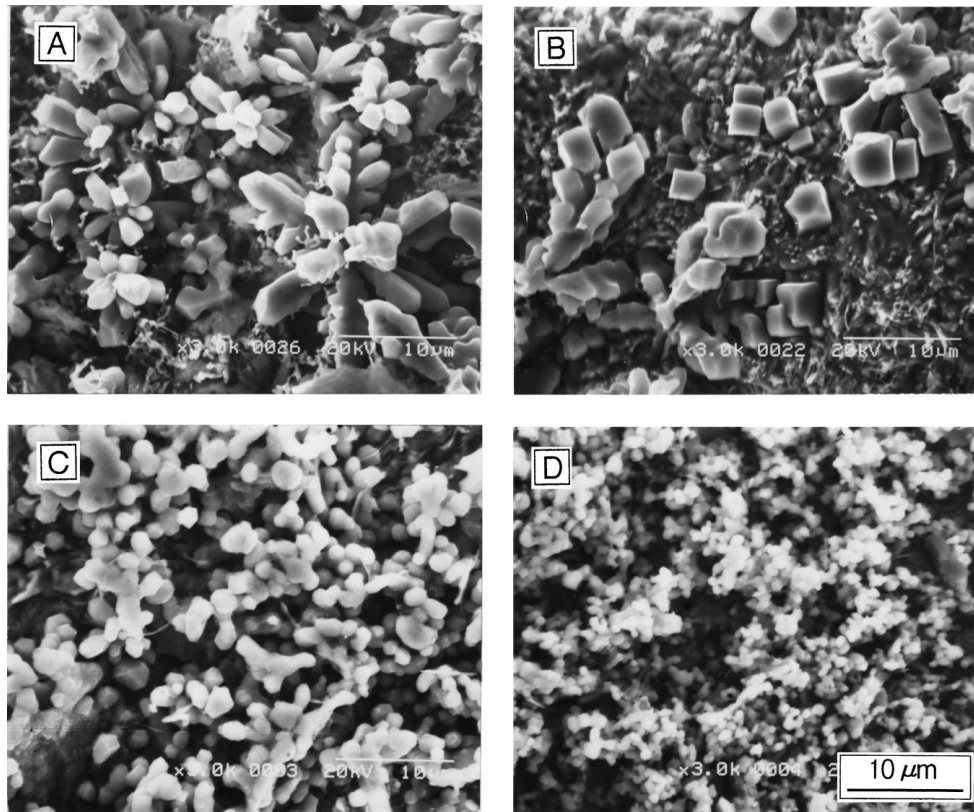


Figure 11 Dendritic morphologies of TiC in the titanium alloyed layer, etched by $\text{HNO}_4 + \text{HF} + \text{H}_2\text{O}$ solution. (A, B): Typical dendritic morphologies at the upper part of alloyed zone. (C, D): Grape-like dendrites near the fusion boundary.

extract during wear processes. Therefore the dendritic TiC morphology is expected to decrease the degradation of wear resistance by the extraction of TiC or severe abrasion of counterpart caused by extracted TiC.

3.5. Hardness profile

Microhardness profile of the as-laser titanium alloyed specimen was compared to that of the heat treated one in GT50 and in GT100 (see Fig. 12). In case of GT50, microhardness was MHV 400–500 in the TiC precipitate zone, MHV 650–900 in the TiC + ledeburite mixed zone and MHV 400–500 in the TiC precipitate zone and MHV 650–900 in the ledeburite zone. The TiC + ledeburite mixed zone was very narrow and the width was only $50 \mu\text{m}$ in the GT100. To decompose the ledeburite which showed an abnormally high hardness profile between the alloyed zone and the base metal the specimen was heat-treated in vacuum at 1223 K for 10.8 ks and furnace cooled. As a result, microhardness was reduced to MHV 150–200 by the decomposition of ledeburite to ferrite and temper carbon, and then the smooth hardness profile was made by reducing the hardness gradually from the surface to the base metal.

The hardness of the TiC precipitate zone was changed a little by heat treatment, while the hardness in the TiC + ledeburite mixed zone decreased to MHV 450–550 by heat treatment from MHV 650–900 at the as-laser alloyed state due to the decomposition of ledeburite.

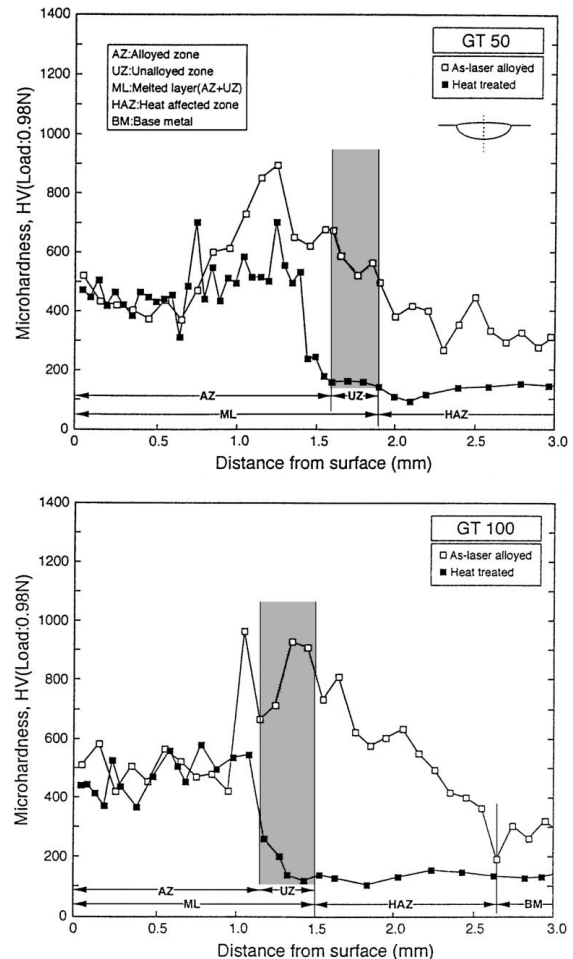


Figure 12 Microhardness profile comparison of as-laser alloyed layer with heat treated layer for GT50 and GT100 respectively.

4. Summary

To examine the possibility of producing a wear resistant TiC particulate composite layer in the cast iron, titanium alloyed bead was produced by CO₂ laser irradiation with a titanium coating on the cast iron substrate. From the results, conclusions can be drawn as follows:

1. When the dendrite arm spacing (λ) measured from the ledeburite in the remelted bead of cast iron substrate was calculated by the Kurobe equation the cooling rate of bead was 1.15×10^4 k/s at traveling speeds of 0.83 mm/s and 10.97×10^4 k/s at 5.00 mm/s. Therefore, the cooling rate used in this study can be assumed to be between 1×10^4 k/s and 1×10^5 k/s in that order.

2. In case of titanium alloyed bead, at the laser beam traveling speeds of 0.83 mm/s or 1.67 mm/s there were a few small pores in the bead surface, while large pores were generated in bead surface at traveling speeds higher than 3.33 mm/s and at 5.00 mm/s sponge-like pores were generated.

3. The microstructure of the alloyed layer consisted of three zones, the TiC particulate precipitate zone, the mixed zone of TiC + ledeburite and the ledeburite zone. TiC particulate was formed by direct reaction between carbon originally contained in cast iron and titanium alloyed by laser remelting of the titanium thermal sprayed coating on the cast iron.

4. TiC particulates were precipitated in the typical dendritic morphology. In the slowly solidified zone of bead, the secondary TiC dendrite arm was grown to cubic crystal of TiC. On the other hand, in the rapidly solidified zone near fusion boundary, the dendrite of TiC particulate was not fully grown and fine granular TiC particulates were grouped like grapes.

5. In case of GT50, the hardness was MHV 400–500 in the TiC precipitate zone, MHV 650–900 in the TiC + ledeburite mixed zone and MHV 500–700 in the ledeburite zone. When decomposition heat treatment of ledeburite was applied, there was little change of the hardness in the TiC particulate precipitate zone while the hardness in the TiC + ledeburite mixed zone and the ledeburite zone were reduced to MHV 450–550 and

MHV 150–200 respectively. Thus, this heat treatment caused a smooth hardness profile in cross section of the alloyed bead.

Acknowledgements

The authors wish to thanks to Mr. R. Nagayama and Mr. T. Ohno who assisted to plasma spraying in the Joining and Welding Research Institute of Osaka University.

References

1. R. ELLIOTT, "Cast Iron Technology" (Butterworths, 1989) p.102.
2. C. W. DAPER and J. M. POATE, *Int. Metal Review* **30** (1985) 85.
3. K. TAKASE, *J. of JSME* **96** (1993) 590.
4. K. NAKATA, *J. of the Japan Soc. for Heat Treatment* **2** (1995) 99.
5. K. NAKATA and S. TOMIDA, *J. of the Japan Institute of Light Metals* **45** (1995) 578.
6. P. A. MOLIAN and H. S. RAJASEKGARA, *Surface Engineering* **2** (1986) 269.
7. K. P. KOOPER and J. D. AYERS, *ibid.* **1** (1985) 263.
8. H. UMEHARA, *Bulletin of the Japan Institute of Metals* **27** (1988) 766.
9. M. TSUJIKAWA *et al.*, *Imono* **64** (1992) 613.
10. NIKKEI MECHANICAL **468** (1995) 24.
11. F. D. SEAMAN and D. S. GNAMUTHU, *Metal Progress* (1975) 67.
12. H. W. BERGMANN, *Surface Engineering* **1** (1985) 137.
13. W. J. TOMLINSON and A. S. BRANSDEN, *ibid.* **6** (1990) 281.
14. M. TSUJIKAWA *et al.*, *J. of Japan Foundry Eng. Soc.* **68** (1996) 657.
15. J. KUROBE *et al.*, *ISIJ* **75** (1989) 102.
16. T. R. ANTHONY and H. E. CLINE, *J. of Applied Physics* **48** (1977) 3888.
17. B. MARINEKI, *Modern Casting* **42** (1963) 99.
18. Y. TAKATA *et al.*, *Imono* **60** (1985) 332.
19. J. MACKOWIAK, "Physical Chemistry for Metallurgy" (George Allen and Unwin, 1966) p. 160.
20. H. TAMURA, *J. of the Japan Welding Soc.* **38** (1969) 117.
21. A. OHONO, "The Solidification of Metals" (Chijin Shokan, Tokyo, 1976) p. 42.

Received 30 May 1997

and accepted 22 July 1999